

# Bayesian Spatial Homogeneity Pursuit of Functional Data: an Application to the U.S. Income Distribution

Guanyu Hu   Junxian Geng   Yishu Xue   Huiyan Sang

June 15, 2021

## Abstract

An income distribution describes how an entity's total wealth is distributed amongst its population. A problem of interest to regional economics researchers is to understand the spatial homogeneity of income distributions among different regions. In economics, the Lorenz curve is a well-known functional representation of income distribution. In this article, we propose a mixture of finite mixtures (MFM) model as well as a Markov random field constrained mixture of finite mixtures (MRFC-MFM) model in the context of spatial functional data analysis to capture spatial homogeneity of Lorenz curves. We design efficient Markov chain Monte Carlo (MCMC) algorithms to simultaneously infer the posterior distributions of the number of clusters and the clustering configuration of spatial functional data. Extensive simulation studies are carried out to show the effectiveness of the proposed methods compared with existing methods. We apply the proposed spatial functional clustering method to state level income Lorenz curves from the American Community Survey Public Use Microdata Sample (PUMS) data. The results reveal a number of important clustering patterns of state-level income distributions across US.

**Keywords:** Lorenz Curve; Markov Random Field; Mixture of Finite Mixtures; Spatial Functional Data Clustering

# 1 Introduction

Our study is motivated by an American Community Survey Public Use Microdata Sample (PUMS) data that contains incomes of United States (US) households in year 2017, which can be accessed via the PUMS data registry (<https://www.census.gov/programs-surveys/acs/data/pums.html>). Incomes of households as well as the states they live in are recorded. Our primary goal is to cluster the state level Income Distribution (ID; O’sullivan and Shefrin, 2007), i.e., how a state’s total wealth is distributed amongst its population. In order to clarify the differences between economics term “Income Distribution” and density distribution of household income, we use ID to represent this particular economic term in the rest of the paper. The ID has been a central concern of economic theory since the time of classical economists such as Adam Smith and David Ricardo. While economists have been conventionally concerned with the relationship between factors of production, land, labor, and capita for ID, modern economists now focus more on income inequality. Particularly, a balance between income inequality and economic growth is a desired goal for policy makers. Capturing homogeneity pattern of state level IDs is of great research interest in economic studies, as it will enhance the understanding of income inequality among different regions within a country, and provide policy makers with reference as to issue different policies for the identified regions. In macroeconomics, most governments want to obtain an equitable (fair) distribution of income, which is a crucial element of a functioning democratic society (Mankiw, 2014). In order to obtain this goal, the distribution of income or wealth in an economy is represented by a Lorenz curve (Lorenz, 1905), which is a function showing the proportion of total income assumed by the bottom  $100p\%$  ( $p \in [0, 1]$ ) of the population. Derived from the Lorenz curve, the Gini coefficient is a commonly used measure for income inequality (Gini, 1997), and it has been widely adopted by many international organizations, such as the United Nations and World Bank, to study income inequalities among regions. The Gini coefficient, however, is only a summary measurement of statistical dispersion of ID, and it is non-unique as two Lorenz curves can assume different shapes but still yield the

same Gini value. The Gini index is related to the Lorenz curve as twice the area between the 45-degree line and the Lorenz curve which is insensitive to the changes of the form of the Lorenz curve. Similarly, the Hoover index (Hoover, 1936) is also derived from the Lorenz curve, and suffers from the same non-uniqueness disadvantage.

Thus far, many methods have been introduced to either directly model Lorenz curves or indirectly through the modeling of statistical distribution functions of household income. Popular parametric methods for modeling the density of personal incomes in general use heavy tail distributions, including Pareto (Pareto, 1964), log-normal (Gibrat, 1931), Weibull (Bartels and Van Metelen, 1975), gamma (Bartels and Van Metelen, 1975), and generalized beta distributions (McDonald, 1984; McDonald and Xu, 1995). Nonparametric methods include the commonly used empirical Lorenz curve estimation method and several other extensions that introduce various smoothing techniques (Ryu and Slottje, 1996; Cowell and Victoria-Feser, 2008). Most of these existing methods only focus on modeling a univariate personal ID. There is a need for the development of spatial functional data analysis techniques to jointly model Lorenz curves across counties or states in economic studies. Without spatial homogeneity pattern detection, each state needs to make its own policy, which could be a waste of public resource, while with a few clusters of states, only (the number of clusters) policies need to be made accordingly.

There are several major challenges in developing clustering algorithms for spatial functional data. First, spatial functional data such as state-level Lorenz curves often exhibit strong location-related patterns. It is necessary to incorporate such spatial structure into spatial functional data clustering algorithms. Nevertheless, most existing functional clustering algorithms are designed under the assumption that the observed functions are i.i.d curves (e.g., see a review paper by Jacques and Preda, 2014). These methods can be broadly classified into three paths: two-stage methods that reduce the dimension by basis representations before applying clustering approaches, nonparametric methods that define specific dissimilarities among functions followed by heuristics or geometric procedures-based cluster-

ing algorithms such as  $K$ -means, and model-based methods that specify clustering models such as mixture of Gaussian for basis coefficients. Recently, a number of works have been proposed to extend these functional clustering algorithms to the spatial context. [Romano et al. \(2011\)](#) and [Giraldo et al. \(2012\)](#) followed the second path to define dissimilarities among spatial functions based on spatial variograms and cross-variograms. [Jiang and Serban \(2012\)](#) followed the third path to model cluster memberships using an auto-regressive Markov random field, and introduce spatially dependent random errors in the conditional model for functions.

Second, it is desired to impose certain spatial contiguous constraints on the clustering configuration to facilitate interpretations in the spatial context. In other words, a local cluster is expected to contain spatially connected components with flexible shapes and sizes. In addition, in many economics applications, this spatial contiguous constraint may not dominate the clustering configuration globally, in the sense that two clusters that are spatially disconnected may still belong to the same cluster. For example, New England area could share certain similar demographic information with California despite the distance in between. Although a large body of model based spatial clustering approaches have been proposed in various spatial contexts, to the best of our knowledge, there is still a lack of clustering methods that allow for both locally spatially contiguous clusters and globally discontinuous clusters. For example, existing Bayesian spatial clustering methods based on mixture models, such as the finite mixture model used in the aforementioned spatial functional clustering algorithm ([Jiang and Serban, 2012](#)), can introduce spatial dependence in cluster memberships but may not fully guarantee spatial contiguity. [Suarez et al. \(2016\)](#) clustered each signal coefficient in a multiresolution wavelet basis using conditionally independent Dirichlet process priors. Among the methods that guarantee spatial contiguity, they may either impose certain constraints on cluster shapes ([Knorr-Held and Raßer, 2000](#); [Kim et al., 2005](#); [Lee et al., 2017](#)), or fail to allow for globally discontinuous clusters ([Li and Sang, 2019](#)).

Finally, an important consideration in clustering is how to determine the number of clusters. Most existing methods such as [Heaton et al. \(2017\)](#) require specification of the number of clusters first. In Bayesian statistics, Dirichlet Process mixture models (DPM) have gained large popularity because of their flexibility in allowing for an unknown number of clusters. Recently, [Miller and Harrison \(2018\)](#) proved that DPM can produce an inconsistent estimate of the number of clusters, and proposed a mixture of finite mixtures model to resolve the issue while inheriting many attractive mathematical and computational properties of DPM. However, their method may not be efficient for spatial clustering as it does not take into account any spatial information.

To address these challenges when facing the analysis of spatial income Lorenz curves, in this article, we develop a new Bayesian nonparametric method that combines the ideas of Markov random field models and mixture of finite mixtures models to leverage geographical information. A distinction of the method is its ability to capture both locally spatially contiguous clusters and globally discontinuous clusters. Moreover, it utilizes an efficient Markov chain Monte Carlo (MCMC) algorithm to estimate the number of clusters and clustering configuration simultaneously while avoiding complicated reversible jump MCMC or allocation samplers. We introduce this new Bayesian nonparametric clustering model to the analysis of the US state level household income Lorenz curves. In particular, we use a similarity measure among functional curves based on the inner product matrix under elastic shape analysis ([Srivastava and Klassen, 2016](#)), which has a nice invariance property to shape-preserving transformations. The results of real data reveal interesting clustering patterns of IDs among different states, which provide important information to study regional income inequalities.

The rest of this paper is organized as follows. The motivating PUMS data is introduced in detail in Section 2. We briefly review elastic shape analysis of functions in Section 3.1, followed by a review of nonparametric Bayesian clustering methods in Section 3.1. We describe the proposed Markov random field constrained mixture of finite mixture prior model

and introduce our functional data clustering model in Section 3.3. In Section 4, the Bayesian inference including the MCMC sampling algorithm, the model selection criterion for tuning parameter, post-MCMC inference, and convergence diagnostic criteria are introduced. Simulation and case study using the PUMS data are presented respectively in Sections 5 and 6. Section 7 closes the paper with some conclusions and discussions.

## 2 Motivating Data

Our motivating data comes from the 2018 submission in the PUMS data registry. US households' incomes and the states they live in are recorded for the 50 states plus Washington, DC. For simplicity, we refer to them as “51 states” in the rest of this paper. The Lorenz curve (Lorenz, 1905) is a commonly used functional representation of the distribution of income or wealth, which reflects inequality of the wealth distribution. It, specifically, assumes that the household income  $x$  follows a cumulative distribution function (CDF)  $F(x)$  with respective probability density function  $f(x)$ . Let  $Q(p) = F^{-1}(p)$  be the inverse CDF defined as  $Q(p) = \inf\{y : F(y) \geq p\}$ . The Lorenz curve is defined as

$$L(p) = \frac{1}{\mu} \int_0^p Q(t) dt, \quad \text{for } 0 \leq p \leq 1,$$

where  $\mu = \int_0^1 Q(t) dt$ . By definition, when plotted in a graph, the Lorenz curve always starts at  $(0,0)$  and ends at  $(1,1)$ , and measures on the bottom for  $100p\%$  of households, what percentage  $100L\%$  of total income they have.

In practice, the empirical Lorenz curve can be constructed from data in a similar fashion using the empirical CDF. Define for state  $i$

$$\widehat{L}_i(p_k) = \sum_{j=1}^k y_{i,(j)} / \sum_{j=1}^T y_{i,(j)},$$

where  $p_k = k/n$ , for  $k = 1, \dots, n$ , and  $y_{i,(j)}$  is the  $j$ -th order statistic observed in state  $i$ .

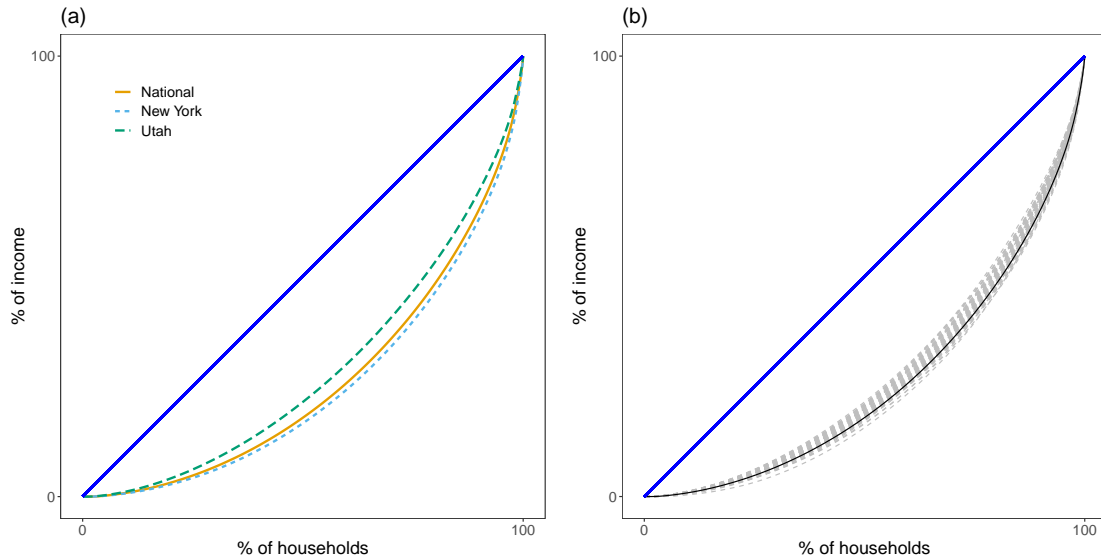


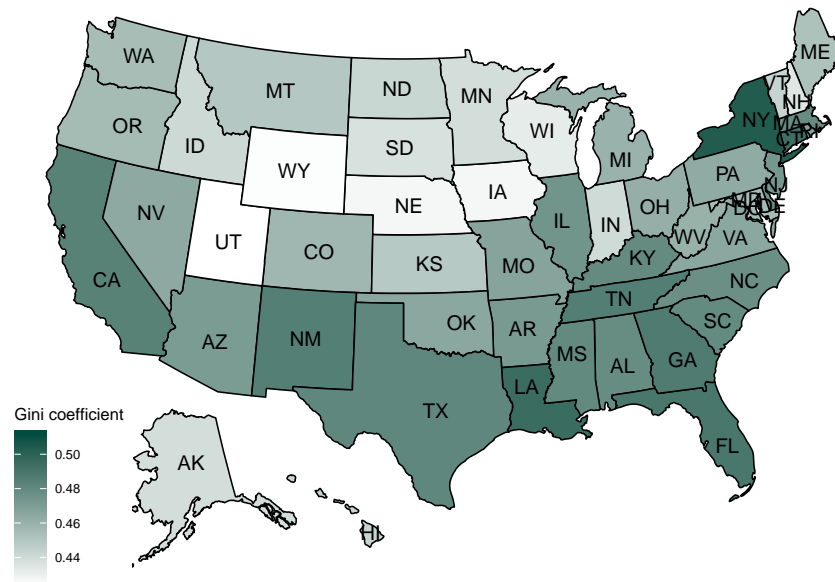
Figure 1: (a) Lorenz curves calculated based on the PUMS 2017 Household Income data on the national level and for two selected states; (b) Lorenz curves for all US states.

Under mild regularity conditions,  $\widehat{L}_i$  converges uniformly in  $p \in [0, 1]$  and almost surely to  $L_i$  (Gastwirth, 1972). The Gini index, as a derived measure, is defined as two times the area between the Lorenz curve and the 45 degree line of equality from  $(0, 0)$  to  $(1, 1)$ .

For the 2017 US household income data, examples of Lorenz curves are presented in Figure 1. The Lorenz curve computed on the national level using all observations is marked in solid line, with a corresponding Gini coefficient of 0.4804. A closer look at the state-level Lorenz curves, however, reveals that the IDs do vary across states. The Lorenz curves for two selected states, Utah and New York, are also illustrated in Figure 1(a) as an example. It is rather apparent that while Utah’s curve lies above the national curve, indicating more equality, New York’s curve lies below, suggesting a larger gap between rich and poor. Lorenz curves for all US states are plotted together with the national curve in Figure 1(b), and they form a “cloud” instead of being similar to each other. The ability of Lorenz curves to describe income inequalities is clearly demonstrated here.

In addition to the Lorenz curves, descriptive statistics, which include the Gini coefficient and state median income, are presented in Figure 2. With a Gini of 0.423, Utah becomes the state that has the least income inequality, and Washington, DC has the worst income

(a)



(b)

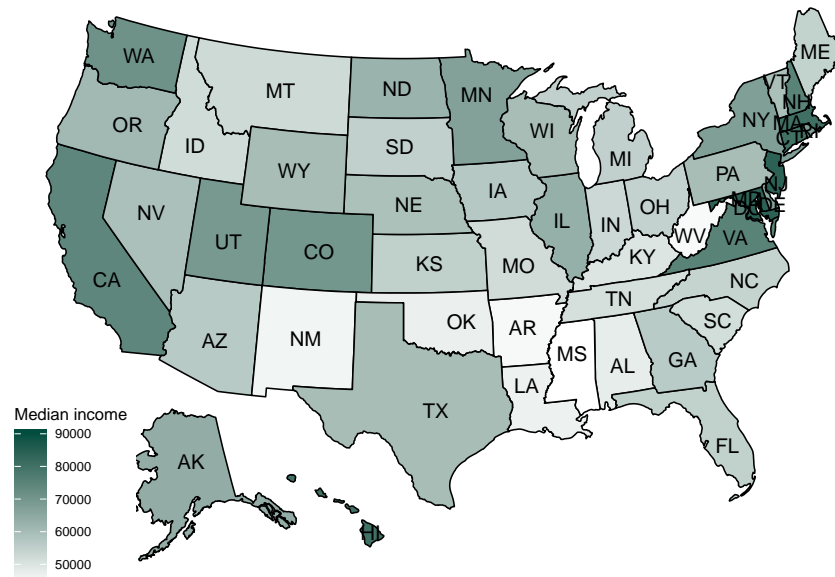


Figure 2: Descriptive statistics of PUMS data on the US map: (a) Gini coefficient; (b) state median income.



inequality with a Gini of 0.512. It also has the highest median income of \$90,000, while Mississippi has the lowest median income of \$43,500.

### 3 Methodology

In this section, we treat the state-level Lorenz curves as spatial functional data. We will first discuss the functional representation of ID and the shape-based similarity measure between two IDs. Next, the nonparametric Bayesian approach for functional data clustering based on the similarity measure is introduced. In addition, a Markov random fields constraint mixture of finite mixtures model (MRFC-MFM) is proposed to add a spatial constraint in clustering prior. The hierarchical model under MRFC-MFM is presented at the end of this section.

#### 3.1 Functional Representation of Income Distribution

We begin the section by reviewing the functional data shape analysis technique. In order to cluster functional data, we need to define appropriate metrics to quantify similarities among functional curves. There are four important features of functional data including quantity, frequency, similarity, and smoothness. Commonly used distance metrics such as the Euclidean distance are no longer appropriate candidates for quantifying similarities between functions. In this article, we consider the inner product matrix calculated using a specific representation of curves called the square-root velocity function (SRVF; [Srivastava et al., 2010](#)). This inner product matrix is a summary statistic that encodes the similarity information among curves for subsequent clustering analysis. This inner product matrix will focus more on the differences between the shape of functions. By focusing on shapes, one is more interested in the numbers and relative heights of peaks and valleys in a curve, rather than their precise locations. This property will be more suitable for quantifying the differences of IDs among different regions, because the precise locations or mean shifts have less effects on inequality of ID.

The SRVF of an absolutely continuous function  $f(t) : [0, 1] \rightarrow \mathcal{R}^p$  is defined as:

$$q(t) = \text{sign}(f'(t)) \sqrt{|f'(t)|}, \quad (3.1)$$

where  $f'(t)$  is the first order derivative of function  $f$  on  $t$ . It can be seen that the SRVF is a curve of unit length. There are several advantages of using SRVF for functional data analysis. First, the scaling, rotation and re-parameterization variabilities still remain based on SRVF. In addition, the elastic metric is invariant to the reparameterization of functions. The SRVF represents unit-length curves as a unit hypersphere in the Hilbert manifold. The SRVF for a given function can be obtained in R using the `f_to_srvf()` function provided by the `fdasrvf` package (Tucker, 2019). For given functions  $f_1$  and  $f_2$  which belong to  $\mathcal{F} = \{f : [0, 1] \rightarrow \mathcal{R}^p : f \text{ is absolutely continuous}\}$  and their corresponding SRVFs,  $q_1$  and  $q_2$ , the inner product is defined based on the definition in Zhang et al. (2015) as follows:

$$S_{f_1, f_2} = \sup_{\gamma \in \Gamma, O \in SO(p)} \langle q_1, (q_2, (O, \gamma)) \rangle, \quad (3.2)$$

where  $SO(p)$  is the collection of orthogonal  $p \times p$ , i.e.  $p$ -dimensional rotation matrices, and  $\Gamma$  represents the set of all orientation-preserving diffeomorphisms over the domain  $[0, 1]$ . The notation  $(O, \gamma)$  denotes a joint action of the rotation and reparameterization operations, and  $(q_2, (O, \gamma))$  here represents certain reparameterizations and rotations of  $q_2$ . The maximization over  $SO(p)$  and  $\Gamma$  can be performed iteratively as in Srivastava et al. (2010). The operation  $\langle \cdot, \cdot \rangle$  denotes the inner product in  $\mathbb{L}^2([0, 1], \mathbb{R}^p)$ :  $\langle v, q \rangle = \int_0^1 \langle v(t), q(t) \rangle dt$ . The value of the integral ranges from  $-1$  to  $1$ , with  $-1$  indicating that the curves are exactly the opposite, and  $1$  indicating that they are exactly the same. The inner product of two functions can be calculated using the algorithm in Tucker et al. (2013). Computation in R is facilitated with the `trapz()` function in package `pracma` (Borchers, 2019). Given  $f_1, \dots, f_n$ , the  $n \times n$  pairwise inner product matrix  $\mathbf{S}$  can be calculated using the definition in (3.2), and `fdasrvf` and `pracma`.

## 3.2 Mixture of Finite Mixtures for Distances Between Functional Data

Next, we introduce nonparametric Bayesian methods to capture spatial homogeneity of functional data. We start with a Fisher's  $Z$ -transformation of the inner product matrix  $\mathbf{S}$  to make each entry  $\mathbf{S}_{f_i, f_j}$  of the matrix within the range of a Gaussian distribution. The transformed inner product matrix is denoted as  $\mathfrak{S}$ , with each entry being

$$\mathfrak{S}_{ij} = \log \left( \frac{1 + \mathbf{S}_{f_i, f_j}}{1 - \mathbf{S}_{f_i, f_j}} \right).$$

The larger  $\mathfrak{S}_{ij}$  is, the closer  $f_i$  and  $f_j$  are. We further assume that

$$\begin{aligned} \mathfrak{S}_{ij} \mid \boldsymbol{\mu}, \boldsymbol{\tau}, k &\sim \text{N}(\mu_{ij}, \tau_{ij}^{-1}), \quad \mu_{ij} = U_{z_i z_j} \\ \tau_{ij} &= T_{z_i z_j}, \quad 1 \leq i \leq j \leq n, \end{aligned} \tag{3.3}$$

where  $k$  is the number of true underlying clusters,  $\text{N}()$  denotes the normal distribution,  $z_i \in \{1, \dots, k\}$  denotes the cluster membership of the  $i$ -th curve;  $\mathbf{U} = [U_{rs}] \in (-\infty, +\infty)^{k \times k}$  and  $\mathbf{T} = [T_{rs}] \in (0, +\infty)^{k \times k}$  are symmetric matrices, with  $U_{rs} = U_{sr}$  indicating the mean closeness of any function  $f_i$  in cluster  $r$  and any function  $f_j$  in cluster  $s$ , and  $T_{rs} = T_{sr}$  indicating the precision of closeness between any function  $f_i$  in cluster  $r$  and any function  $f_j$  in cluster  $s$ . Note that in the above formulation, only the upper triangle of matrix  $\mathfrak{S}$  is modeled, including the diagonal.

Let  $\mathcal{Z}_{n,k} = \{(z_1, \dots, z_n) : z_i \in \{1, \dots, k\}, 1 \leq i \leq n\}$  denote all possible partitions of  $n$  nodes into  $k$  clusters. Given  $z \in \mathcal{Z}_{n,k}$ , let  $\mathfrak{S}_{[rs]}$  denote the  $n_r \times n_s$  sub-matrix of  $\mathfrak{S}$  consisting of entries  $\mathfrak{S}_{ij}$  with  $z_i = r$  and  $z_j = s$ . Following the common practice for stochastic block models (SBM; [Holland et al., 1983](#)), independence between entries of  $\mathfrak{S}$ , or edges, is assumed.

The joint likelihood of  $\mathcal{S}$  under model (3.3) can be expressed as

$$\begin{aligned}
P(\mathcal{S} \mid \mathbf{z}, \mathbf{U}, \mathbf{T}, k) &= \prod_{1 \leq r \leq s \leq k} P(\mathcal{S}_{[rs]} \mid \mathbf{z}, \mathbf{U}, \mathbf{T}), \\
P(\mathcal{S}_{[rs]} \mid \mathbf{z}, \mathbf{U}, \mathbf{T}) &= \prod_{1 \leq i < j \leq n: z_i=r, z_j=s} \frac{1}{\sqrt{2\pi T_{rs}^{-1}}} \exp \left\{ -\frac{T_{rs}(\mathcal{S}_{ij} - U_{rs})^2}{2} \right\}.
\end{aligned} \tag{3.4}$$

A common Bayesian specification when  $k$  is given can be completed by assigning independent priors to  $\mathbf{z}$ ,  $\mathbf{U}$  and  $\mathbf{T}$ , and it can be easily incorporated into a framework as finite mixture models. A popular solution for unknown  $k$  is to introduce the Dirichlet process mixture prior models (Antoniak, 1974) as following:

$$\mathcal{S}_i \sim F(\cdot, \boldsymbol{\theta}_i), \quad \boldsymbol{\theta}_i \sim G(\cdot), \quad G \sim DP(\alpha G_0), \tag{3.5}$$

where  $\mathcal{S}_i = (\mathcal{S}_{i1}, \mathcal{S}_{i2}, \dots, \mathcal{S}_{in})$ ,  $\boldsymbol{\theta}_i = (\boldsymbol{\theta}_{i1}, \boldsymbol{\theta}_{i2}, \dots, \boldsymbol{\theta}_{in})$  and  $\boldsymbol{\theta}_{ij} = (\mu_{ij}, \tau_{ij})$ .

Dirichlet process is parameterized by a base measure  $G_0$  and a concentration parameter  $\alpha$ . If a set of values of  $\boldsymbol{\theta}_1, \dots, \boldsymbol{\theta}_n$  are drawn from  $G$ , a conditional prior can be obtained by integration (Blackwell et al., 1973):

$$p(\boldsymbol{\theta}_{n+1} \mid \boldsymbol{\theta}_1, \dots, \boldsymbol{\theta}_n) = \frac{1}{n + \alpha} \sum_{i=1}^n \delta_{\boldsymbol{\theta}_i}(\boldsymbol{\theta}_{n+1}) + \frac{\alpha}{n + \alpha} G_0(\boldsymbol{\theta}_{n+1}). \tag{3.6}$$

Here,  $\delta_{\boldsymbol{\theta}_i}(\boldsymbol{\theta}_j) = I(\boldsymbol{\theta}_j = \boldsymbol{\theta}_i)$  is the distribution concentrated at a single point  $\boldsymbol{\theta}_i$ . Equivalent models can also be obtained by introducing cluster membership  $z_i$ 's and letting the unknown number of clusters  $K$  go to infinity (Neal, 2000).

$$\begin{aligned}
\mathcal{S}_i \mid z_i, \boldsymbol{\theta}^* &\sim F(\boldsymbol{\theta}_{z_i}^*), \\
z_i \mid \boldsymbol{\pi} &\sim \text{Discrete}(\pi_1, \dots, \pi_K), \\
\boldsymbol{\theta}_c^* &\sim G_0 \\
\boldsymbol{\pi} &\sim \text{Dirichlet}(\alpha/K, \dots, \alpha/K)
\end{aligned} \tag{3.7}$$

where  $\boldsymbol{\pi} = (\pi_1, \dots, \pi_K)$ . For each cluster  $c$ , the parameters  $\boldsymbol{\theta}_c^*$  determine the cluster specific distribution  $F(\cdot \mid \boldsymbol{\theta}_c^*)$ .

By integrating out mixing proportions  $\boldsymbol{\pi}$ , we can obtain the prior distribution of  $(z_1, z_2, \dots, z_n)$  that allows for automatic inference on the number of clusters  $k$ , which is also well known as the Chinese restaurant process (CRP; Aldous, 1985; Pitman, 1995; Neal, 2000). Through the popular Chinese restaurant metaphor,  $z_i$ ,  $i = 2, \dots, n$  are defined through the following conditional distribution (Pólya urn scheme, Blackwell et al., 1973):

$$P(z_i = c \mid z_1, \dots, z_{i-1}) \propto \begin{cases} |c|, & \text{at an existing table labeled } c \\ \alpha, & \text{if } c \text{ is a new table} \end{cases}, \quad (3.8)$$

where  $|c|$  is the size of cluster  $c$ .

While the CRP has a very attractive feature of simultaneous estimation on the number of clusters and the cluster configuration, a striking limitation of this model has been recently discovered. Miller and Harrison (2018) proved that the CRP produces extraneous clusters in the posterior leading to inconsistent estimation of the *number of clusters* even when the sample size grows to infinity. A modification of the CRP called mixture of finite mixtures (MFM) model is proposed to circumvent this issue (Miller and Harrison, 2018):

$$k \sim p(\cdot), \quad (\pi_1, \dots, \pi_k) \mid k \sim \text{Dirichlet}(\gamma, \dots, \gamma), \quad z_i \mid k, \boldsymbol{\pi} \sim \sum_{h=1}^k \pi_h \delta_h, \quad i = 1, \dots, n, \quad (3.9)$$

where  $p(\cdot)$  is a proper probability mass function (p.m.f.) on  $\{1, 2, \dots\}$  and  $\delta_h$  is a point-mass at  $h$ . Compared to the CRP, the introduction of new tables is slowed down by the factor  $V_n(w+1)/V_n(w)$ , which facilitates a model-based pruning of the tiny extraneous clusters. The coefficient  $V_n(w)$  needs to be precomputed as:

$$V_n(w) = \sum_{k=1}^{+\infty} \frac{k^{(w)}}{(\gamma k)^{(n)}} p(k),$$

where  $k_{(w)} = k(k-1)\dots(k-w+1)$ , and  $(\gamma k)^{(n)} = \gamma k(\gamma k+1)\dots(\gamma k+n-1)$ . By convention,  $x^{(0)} = 1$  and  $x_{(0)} = 1$ .

The conditional prior of  $\boldsymbol{\theta}$  under MFM can be stated as below:

$$P(\boldsymbol{\theta}_{n+1} \mid \boldsymbol{\theta}_1, \dots, \boldsymbol{\theta}_n) \propto \sum_{i=1}^w (n_i + \gamma) \delta_{\boldsymbol{\theta}_i^*} + \frac{V_n(w+1)}{V_n(w)} \gamma G_0(\boldsymbol{\theta}_{n+1}). \quad (3.10)$$

where  $\boldsymbol{\theta}_1^*, \dots, \boldsymbol{\theta}_w^*$  are the distinct values taken by  $\boldsymbol{\theta}_1, \dots, \boldsymbol{\theta}_n$  and  $w$  is the number of existing clusters. The cluster membership  $z_i$ , for  $i = 2, \dots, n$ , in (3.9) can be defined in a Pólya urn scheme similar to CRP:

$$P(z_i = c \mid z_1, \dots, z_{i-1}) \propto \begin{cases} |c| + \gamma, & \text{at an existing table labeled } c \\ V_n(w+1)/V_n(w)\gamma, & \text{if } c \text{ is a new table} \end{cases}. \quad (3.11)$$

where  $w$  is the number of existing clusters.

Adapting MFM to our model setting for functional clustering, the model and prior can be expressed hierarchically as:

$$\begin{aligned} k &\sim p(\cdot), \quad \text{where } p(\cdot) \text{ is a p.m.f on } \{1, 2, \dots\} \\ T_{rs} &= T_{sr} \stackrel{\text{ind}}{\sim} \text{Gamma}(\alpha, \beta), \quad r, s = 1, \dots, k, \\ U_{rs} &= U_{sr} \stackrel{\text{ind}}{\sim} \text{N}(\mu_0, k_0^{-1} T_{rs}^{-1}), \quad r, s = 1, \dots, k, \\ \text{pr}(z_i = j \mid \boldsymbol{\pi}, k) &= \pi_j, \quad j = 1, \dots, k, \quad i = 1, \dots, n, \\ \boldsymbol{\pi} \mid k &\sim \text{Dirichlet}(\gamma, \dots, \gamma), \\ \mathcal{S}_{ij} \mid \boldsymbol{z}, \boldsymbol{U}, \boldsymbol{T}, k &\stackrel{\text{ind}}{\sim} \text{N}(\mu_{ij}, \tau_{ij}^{-1}), \quad \mu_{ij} = U_{z_i z_j}, \quad \tau_{ij} = T_{z_i z_j}, \quad 1 \leq i < j \leq n. \end{aligned} \quad (3.12)$$

We assume  $p(\cdot)$  is a Poisson(1) distribution truncated to be positive through the rest of the paper, which has been proved by [Miller and Harrison \(2018\)](#) and [Geng et al. \(2019\)](#) to guarantee consistency for the mixing distribution and the number of clusters. We refer to

the hierarchical model in (3.12) as MFM-fCluster.

### 3.3 Markov Random Field Constrained MFM in Functional data

A possible weakness of MFM for spatial functional data is due to its inability to account for spatial structure or dependence, i.e., MFM neglects the spatial smoothness of a map, and hence the resulting clustering does not comply any spatial constraints, and therefore might be sensitive to noise in the data. This drawback can be addressed by introducing spatial coupling between adjacent features. Applying a Markov random field prior to spatial statistical modeling is a classical Bayesian approach widely used in image segmentation problems (Geman and Geman, 1984). In this section, we combine the similar idea of Markov random fields with MFM to introduce spatial constraints for clustering.

The Markov random field (MRF; Orbanz and Buhmann, 2008) provides a convenient approach to address the difficult problem of modeling a collection of dependent random variables (Winkler, 2012). The dependence structure of different states can be represented by a graph, with vertices representing random variables and an edge between two vertices indicating statistical dependence, which can conveniently introduce the spatial smoothness for both Gaussian and non-Gaussian data (e.g., mixture data). Interactions among variables are constrained to a small group that are usually assumed to be closer spatially, in order to reduce the complexity of the problem. The neighborhood dependence structure of MRF is encoded by a weighted graph  $\mathcal{N} = (V_{\mathcal{N}}, E_{\mathcal{N}}, W_{\mathcal{N}})$  in space, with vertices  $V_{\mathcal{N}} = (v_1, \dots, v_n)$  representing random variables at  $n$  spatial locations,  $E_{\mathcal{N}}$  denoting a set of edges representing statistical dependence among vertices, and  $W_{\mathcal{N}}$  denoting the edge weights representing the magnitudes of dependence.

The MRF for a collection of random variables  $\boldsymbol{\theta}_1, \dots, \boldsymbol{\theta}_n$  on a graph  $\mathcal{N}$  has a valid joint distribution  $M(\boldsymbol{\theta}_1, \dots, \boldsymbol{\theta}_n) := \frac{1}{Z_H} \exp\{-H(\boldsymbol{\theta}_1, \dots, \boldsymbol{\theta}_n)\}$ , with  $H$  being the cost function with

the following form

$$H(\boldsymbol{\theta}_1, \dots, \boldsymbol{\theta}_n) := \sum_{A \in \mathcal{C}_N} H_A(\boldsymbol{\theta}_A), \quad (3.13)$$

where  $\mathcal{C}_N$  denotes the set of all cliques in  $\mathcal{N}$ , each term  $H_A$  is a non-negative function over the variables in clique  $A$ , and  $Z_H$  is a normalization term. By Hammersley-Clifford theorem, the corresponding conditional distributions enjoy the Markov property, i.e.,  $M(\boldsymbol{\theta}_i | \boldsymbol{\theta}_{-i}) = M(\boldsymbol{\theta}_i | \boldsymbol{\theta}_{\partial(i)})$ , where  $\partial(i) := \{j | (i, j) \in E_N\}$  denotes the set of neighbors of observation  $i$ . Considering only pairwise interactions, we model the conditional cost functions as

$$H(\boldsymbol{\theta}_i | \boldsymbol{\theta}_{-i}) := -\lambda \sum_{l \in \partial(i)} I(\boldsymbol{\theta}_l = \boldsymbol{\theta}_i) = -\lambda \sum_{l \in \partial(i)} I(z_l = z_i), \quad (3.14)$$

where  $\lambda \in \mathbb{R}^+$  is a parameter controlling the magnitude of spatial smoothness, with larger values inducing stronger spatial smoothing. It can be seen that the function takes value in  $\{0, -\lambda\}$ .

Markov random field constrained MFM (MRFC-MFM) is composed of an interaction term modeled by a MRF cost function to capture spatial interactions among vertices and a vertex-wise term modeled by a MFM. The resulting model defines a valid MRF distribution  $\Pi$ , which can be written as

$$\Pi(\boldsymbol{\theta}_1, \dots, \boldsymbol{\theta}_n) \propto P(\boldsymbol{\theta}_1, \dots, \boldsymbol{\theta}_n) M(\boldsymbol{\theta}_1, \dots, \boldsymbol{\theta}_n) \quad (3.15)$$

with  $P(\boldsymbol{\theta}_1, \dots, \boldsymbol{\theta}_n)$  defined by the conditional distributions in (3.10) and  $M(\boldsymbol{\theta}_1, \dots, \boldsymbol{\theta}_n)$  from the MRF model using (3.14) as the conditional cost function. This constrained model exhibits a key property that the MRF constraints only change the finite component of the MFM model as shown in Theorem 3.1 below. The proof is deferred to Appendix A.

**Theorem 3.1.** *Let  $n_k^{(-i)}$  denote the size of the  $k$ -th cluster excluding  $\theta_i$ ,  $K^*$  denote the number of clusters excluding the  $i$ -th observation, and assume  $H(\theta_i | \theta_{-i})$  is a valid MRF*



conditional cost function. The conditional distribution of a MRFC-MFM takes the form

$$\Pi(\boldsymbol{\theta}_i | \boldsymbol{\theta}_{-i}) \propto \sum_{k=1}^{K^*} (n_k^{(-i)} + \gamma) \frac{1}{Z_H} \exp(-H(\boldsymbol{\theta}_i | \boldsymbol{\theta}_{-i})) \delta_{\boldsymbol{\theta}_k^*}(\boldsymbol{\theta}_i) + \frac{V_n(K^* + 1)}{V_n(K^*)} \frac{\gamma}{Z_H} G_0(\boldsymbol{\theta}_i).$$

An immediate corollary of Theorem 3.1 can be defined in a Pólya urn scheme after introducing the cluster assignments parameters  $z_i, i = 1, \dots, n$ .

**Corollary 1.** *Suppose the conclusion of Theorem 3.1 holds. Then,*

$$\Pi(z_i = c | \mathbf{z}_{-i}) \propto \begin{cases} [|c| + \gamma] \exp\left[\lambda \sum_{l \in \partial(i)} I(z_l = z_i)\right], & \text{at an existing table labeled } c \\ V_n(K^* + 1)/V_n(K^*)\gamma, & \text{if } c \text{ is a new table} \end{cases},$$

where  $\mathbf{z}_{-i} = \mathbf{z} \setminus \{z_i\}$ , i.e., all elements of  $\mathbf{z}$  except for  $z_i$ .

The above scheme offers an intuitive interpretation of MRFC-MFM again using the Chinese restaurant metaphor: the probability of a customer  $i$  sitting at a table depends not only on the number of other customers already sitting at that table, but also the number of other customers that have spatial ties to the  $i$ -th customer. The parameter  $\lambda$  controls the strength of spatial ties, and ultimately controls estimation on the number of clusters. The larger the value for  $\lambda$ , the stronger the spatial smoothing effect and the smaller the number of clusters. This can be clearly observed in the simulation results presented in the sensitivity analysis section of the supplemental material. In particular, the MFM model developed in [Miller and Harrison \(2018\)](#) can be viewed as a special case of MRFC-MFM when  $\lambda = 0$ . We use the notation MRFC-MFM( $\lambda, G_0$ ) to represent the MRFC-MFM prior with a smoothness parameter  $\lambda$  and a base distribution  $G_0$ . The Markov random field constraint-mixture of finite mixture-functional clustering method (MRFC-MFM-fCluster) can be hierarchically

written as

$$\mathbf{U}, \mathbf{T}, \mathbf{z}, k \sim \text{MRFC-MFM}(\lambda, G_0), \quad (3.16)$$

$$\mathcal{S}_{ij} \mid \mathbf{z}, \mathbf{U}, \mathbf{T}, k \stackrel{\text{ind}}{\sim} \text{N}(\mu_{ij}, \tau_{ij}^{-1}), \quad \mu_{ij} = U_{z_i z_j}, \tau_{ij} = T_{z_i z_j} \quad 1 \leq i < j \leq n,$$

where  $G_0$  is a normal-gamma distribution whose hyperparameters are the same with (3.12). It is noted that while the model in (3.16) introduces spatial dependence to promote locally contiguous clustering, it still allows any customer a chance to sit with any other customer so that globally discontinuous clustering can be captured.

## 4 Bayesian Inference

MCMC is used to draw samples from the posterior distributions of the model parameters. In this section we present the sampling scheme, the posterior inference of cluster configurations, and metrics to evaluate the estimation performance and clustering accuracy.

### 4.1 The MCMC Sampling Schemes

Our goal is to sample from the posterior distribution of the unknown parameters  $k$ ,  $\mathbf{z} = (z_1, \dots, z_n) \in \{1, \dots, k\}^n$ ,  $\mathbf{U} = [U_{rs}] \in (-\infty, +\infty)^{k \times k}$  and  $\mathbf{T} = [T_{rs}] \in (0, +\infty)^{k \times k}$ . While inference in MFMs can be done with methods such as reversible jump Markov chain Monte Carlo or even allocation samplers, they often suffer from poor mixing and slow convergence. We adapt the algorithm in [Miller and Harrison \(2018\)](#) to exploit the Pólya urn scheme for the MRFC-MFM. An efficient collapsed Gibbs sampler is used for Bayesian inference by marginalizing out  $k$  analytically. The sampler for MFM is presented in Algorithm 1 in the supplemental material, and the sampler for MRFC-MFM is presented in Algorithm 2 in the supplemental material. These two algorithms only differ by the posterior probability of an observation assigned to an existing cluster. Both algorithms efficiently cycle through the full

conditional distributions of  $z_i$  given  $\mathbf{z}_{-i}$ ,  $\mathbf{U}$ , and  $\mathbf{T}$  for  $i = 1, 2, \dots, n$ .

For the hyperparameters in both simulation studies and real data analysis, we use  $\alpha = 1$ ,  $\beta = 1$ ,  $k_0 = 2$  and  $\gamma = 1$ . For  $\mu_0$ ,  $\max_{i,j} \mathcal{S}$  is assigned to diagonal terms and  $\min_{i,j} \mathcal{S}$  is assigned to off-diagonal terms in order to make it more informative. The choices of  $\mu_0$  ensure that the functions within a cluster are closer to each other than between clusters. We arbitrarily initialized the algorithms with nine clusters, and randomly allocated the cluster configurations. Various other choices were tested and we did not find any evidence of sensitivity to the initialization.

## 4.2 Post MCMC Inference

Dahl’s method (Dahl, 2006) is a popular post-MCMC inference algorithm for the clustering configurations  $\mathbf{z}$  and the estimated parameters. The inference of Dahl’s method is based on the membership matrices,  $B^{(1)}, \dots, B^{(M)}$ , from the posterior samples. The membership matrix  $B^{(t)}$  for the  $t$ -th post-burn-in MCMC iteration is defined as:

$$B^{(t)} = [B^{(t)}(i, j)]_{i, j \in \{1:n\}} = 1(z_i^{(t)} = z_j^{(t)})_{n \times n}, \quad t = 1, \dots, M, \quad (4.1)$$

where  $1(\cdot)$  denotes the indicator function, i.e.,  $B^{(t)}(i, j) = 1$  indicates observations  $i$  and  $j$  are in the same cluster in the  $t$ -th posterior sample after burn-in iterations. Based on the membership matrices for the posterior samples, an Euclidean mean for membership matrices is calculated by:

$$\bar{B} = \frac{1}{M} \sum_{t=1}^M B^{(t)}.$$

The iteration with the least squared distance to  $\bar{B}$  is obtained by

$$C_{LS} = \operatorname{argmin}_{t \in \{1:M\}} \sum_{i=1}^n \sum_{j=1}^n \{B(i, j)^{(t)} - \bar{B}(i, j)\}^2. \quad (4.2)$$

The estimated parameters, together with the cluster assignments  $\mathbf{z}$ , are then extracted from the  $C_{LS}$ -th post burn-in iteration. An advantage of the Dahl's method is to utilize the information of the empirical pairwise probability matrix  $\bar{B}$ .

Convergence diagnostic of the clustering algorithm is evaluated using the Adjusted Rand index (ARI; [Hubert and Arabie, 1985](#)). As an adjusted version of the Rand Index (RI; [Rand, 1971](#)), it measures the concordance between two clustering schemes, after accounting for chances. Taking values between 0 and 1, a large ARI value indicates high concordance. In particular, when two cluster configurations are identical in terms of modulo labeling of nodes, the ARI takes value 1.

### 4.3 Selection of $\lambda$

In our MRFC-MFM-fCluster algorithm, it is rather important to choose an appropriate value for  $\lambda$ , which controls the magnitude of spatial smoothness. Under the Bayesian framework, the deviance information criterion (DIC; [Spiegelhalter et al., 2002](#)), the Bayesian equivalent of the Akaike information criterion (AIC; [Akaike, 1973](#)), has been one of the most frequently used model selection criterion. The AIC, however, does not exert enough penalization for clustering problems, which often leads to over-clustering results. Therefore, we consider using a modified version of DIC (mDIC), which modifies the magnitude of the penalty term of classic DIC to be the same as the Bayesian information criterion (BIC; [Schwarz et al., 1978](#)). The mDIC is calculated as

$$\text{mDIC} = \text{Dev}(\bar{\theta}) + \log\left(\frac{n \times (n + 1)}{2}\right) p_D, \quad (4.3)$$

where

$$\text{Dev}(\theta) = -2 \log \prod_{1 \leq i < j \leq n: z_i=r, z_j=s} \frac{1}{\sqrt{2\pi T_{rs}^{-1}}} \exp\left\{-\frac{T_{rs}(\mathcal{S}_{ij} - U_{rs})^2}{2}\right\},$$

$\theta = \{1 \leq i < j \leq n : z_i = r, z_j = s, U_{rs}, T_{rs}\}$ , and

$$p_D = \overline{D(\theta)} - D(\bar{\theta}),$$

with  $\bar{\theta}$  being the estimated parameters based on Dahl’s method. The model with smaller value of mDIC is preferred.

## 5 Simulation

In this section, we detail the simulation settings, the evaluation metrics, and the comparison performance results.

### 5.1 Simulation Setting and Evaluation Metrics

We simulate the data using the spatial structure of the 51 states. We consider in total three partition settings with respective true number of clusters 3, 5, and 4. The first partition setting shown in Figure 3 consists of two disjoint parts in the east and west coast. It is designed to mimic a rather common economic pattern that geographically distant regions share similar ID pattern, and geographical proximity is not the sole factor for determining homogeneity in ID. The second setting is the five-cluster partition in Figure 4, where there are more true underlying clusters. The third and final setting has four underlying clusters, and the spatial constraint of clusters is “weaker” than those under the other two designs, composing of many spatially discontinuous states and regions, as shown in Figure 5.

Following Salem and Mount (1974), we generate 10,000 simulated observations for each state from a Gamma distribution to mimic the long-tailed pattern that is often observed in econometrics data. In addition, an additional noise term following a Gamma distribution is added with probability so that the ID within each state does not comprise a perfect fit to one certain distribution. We assume each cluster has its own set of distribution parameters shared by all states within it. The true values of the parameters are set so that the Lorenz

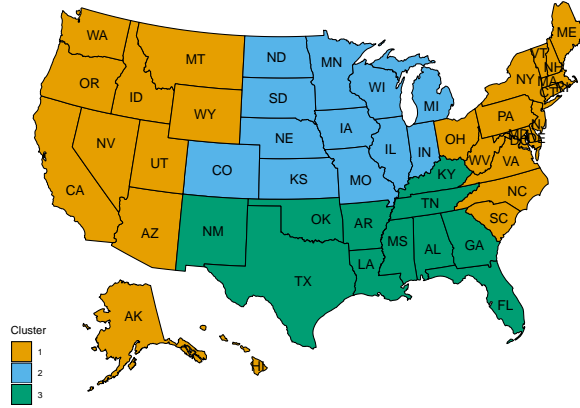


Figure 3: Illustration of the first partition setting with three true clusters, where the first cluster consists of two disjoint components.

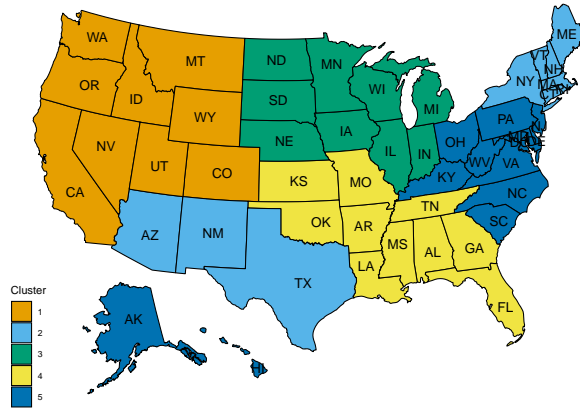


Figure 4: Illustration of the second partition setting with five clusters, where clusters 2 and 5 both have disjoint components.

curves computed on the simulated data are highly similar to those computed from real data (see Table 1). We consider two different parameter settings with small and large differences in income distributions among clusters, corresponding to weak and strong signal designs, respectively. For a total of 100 replicates, we show the Gini indices for different clusters of both weak and strong signal designs in Figure 6, which clearly exhibits major and minor overlapping among clusters, respectively.

The final clustering performance is evaluated using the estimated number of clusters and ARI. The ARI is calculated using the final clustering result selected by Dahl’s method for each replicate, and we calculate an average ARI over all replicates in each setting. Computation

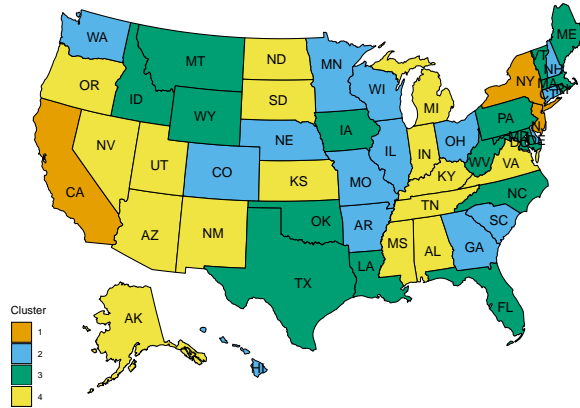


Figure 5: Illustration of the third partition setting with four clusters, where the clusters are composed of disjoint states and regions.

of the ARI is facilitated with the R package `mclust` (Scrucca et al., 2016). In each replicate of simulation, the outcome would be a clustering scheme of 51 states into several clusters. If the number of unique clusters in the scheme for a replicate equals the true number of clusters (3 in the first design, 5 in the second), this replicate is counted towards one time that the number of clusters is correctly inferred. We report the total counts of replicates with correctly inferred number of clusters out of 100 replicates.

## 5.2 Simulation Results

We first examine the inference results of the number of clusters, as well as the accuracy of clustering results from both MFM-fCluster and MRFC-MFM-fCluster. Each parameter setting listed in Table 1 is run with 100 replicates. For MRFC-MFM-fCluster,  $\lambda \in \{0.5, 1, 1.5, 2, 2.5, 3\}$  are considered, and the best  $\lambda$  value is selected using mDIC within each replicate. The graph distance (GD; Bhattacharyya and Bickel, 2014) is used as the distance measure to construct the neighborhood graph used in the Markov random field model. Different upper limits of distance for two states to be considered as “neighbor” are used for the two designs. For the first three-cluster partition, the upper limit is set to 3. For the second five-cluster partition, however, due to the relatively small true cluster sizes, an

Table 1: Simulation designs with weak and strong signals. The symbol  $\Gamma$  denotes Gamma distribution, and “Bin” denotes binomial distribution.

Design	Signal	Cluster	Design
<b>Three Clusters</b>			
	Weak	1	$\Gamma(1.15, 50000) + \text{Bin}(0.05) \cdot \Gamma(0.3, 50000)$
		2	$\Gamma(1.20, 50000) + \text{Bin}(0.05) \cdot \Gamma(0.3, 50000)$
		3	$\Gamma(1.25, 50000) + \text{Bin}(0.05) \cdot \Gamma(0.3, 50000)$
	Strong	1	$\Gamma(1.10, 50000) + \text{Bin}(0.05) \cdot \Gamma(0.5, 50000)$
		2	$\Gamma(1.20, 50000) + \text{Bin}(0.05) \cdot \Gamma(0.5, 50000)$
		3	$\Gamma(1.30, 50000) + \text{Bin}(0.05) \cdot \Gamma(0.5, 50000)$
<b>Five Clusters</b>			
	Weak	1	$\Gamma(1.10, 50000) + \text{Bin}(0.05) \cdot \Gamma(0.3, 50000)$
		2	$\Gamma(1.15, 50000) + \text{Bin}(0.05) \cdot \Gamma(0.3, 50000)$
		3	$\Gamma(1.20, 50000) + \text{Bin}(0.05) \cdot \Gamma(0.3, 50000)$
		4	$\Gamma(1.25, 50000) + \text{Bin}(0.05) \cdot \Gamma(0.3, 50000)$
		5	$\Gamma(1.30, 50000) + \text{Bin}(0.05) \cdot \Gamma(0.3, 50000)$
	Strong	1	$\Gamma(1.00, 50000) + \text{Bin}(0.05) \cdot \Gamma(0.5, 50000)$
		2	$\Gamma(1.10, 50000) + \text{Bin}(0.05) \cdot \Gamma(0.5, 50000)$
		3	$\Gamma(1.20, 50000) + \text{Bin}(0.05) \cdot \Gamma(0.5, 50000)$
		4	$\Gamma(1.30, 50000) + \text{Bin}(0.05) \cdot \Gamma(0.5, 50000)$
		5	$\Gamma(1.40, 50000) + \text{Bin}(0.05) \cdot \Gamma(0.5, 50000)$
<b>Four Clusters</b>			
	Weak	1	$\Gamma(1.15, 50000) + \text{Bin}(0.05) \cdot \Gamma(0.3, 50000)$
		2	$\Gamma(1.20, 50000) + \text{Bin}(0.05) \cdot \Gamma(0.3, 50000)$
		3	$\Gamma(1.25, 50000) + \text{Bin}(0.05) \cdot \Gamma(0.3, 50000)$
		4	$\Gamma(1.30, 50000) + \text{Bin}(0.05) \cdot \Gamma(0.3, 50000)$
	Strong	1	$\Gamma(1.10, 50000) + \text{Bin}(0.05) \cdot \Gamma(0.5, 50000)$
		2	$\Gamma(1.20, 50000) + \text{Bin}(0.05) \cdot \Gamma(0.5, 50000)$
		3	$\Gamma(1.30, 50000) + \text{Bin}(0.05) \cdot \Gamma(0.5, 50000)$
		4	$\Gamma(1.40, 50000) + \text{Bin}(0.05) \cdot \Gamma(0.5, 50000)$



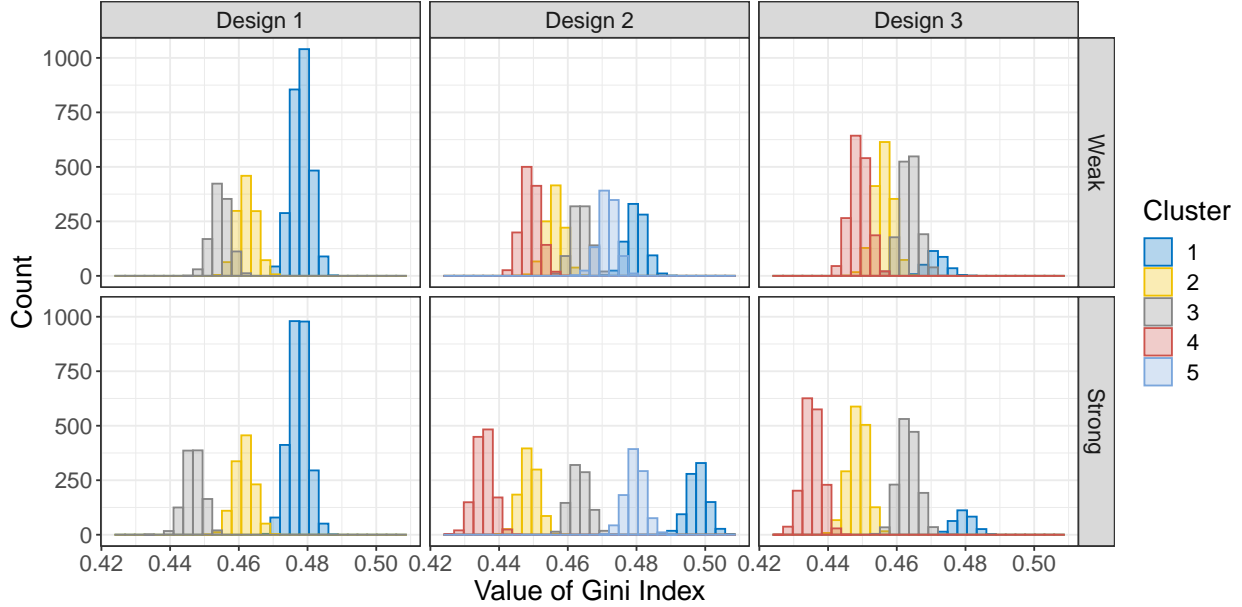


Figure 6: Histograms of Gini indices calculated from the simulated state-wise income data (5,100 in each panel from 100 replicates) for weak and strong signals under the three true partition settings.

upper limit of 1, i.e., only immediate neighbors, is adopted. Similarly, for the third design, as the clusters have more disjoint components, and a state is more likely to have neighbors that belong to a different cluster from its own, we also consider an upper limit of 1.

In addition to MFM-fCluster, we also consider two other competing methods. In the first competing method, we treat the SRVFs derived from Lorenz curves as vectors, and use  $K$ -means to cluster them. The second competing method is the model-based clustering for sparsely sampled functional data proposed by [James and Sugar \(2003\)](#), which is available in R package **fancy**, and can be performed with function `funicit()` with option `method="fitclust"`. Clustering recovery performances of all three methods are measured using ARI. For our proposed method, we present the average of ARIs corresponding to the  $\lambda$  value selected by mDIC in each replicate. As neither  $K$ -means or model-based clustering can estimate the number of clusters but instead require it to be provided, to make a fair comparison, we provide the number of clusters inferred by each replicate corresponding to its selected optimal  $\lambda$ .

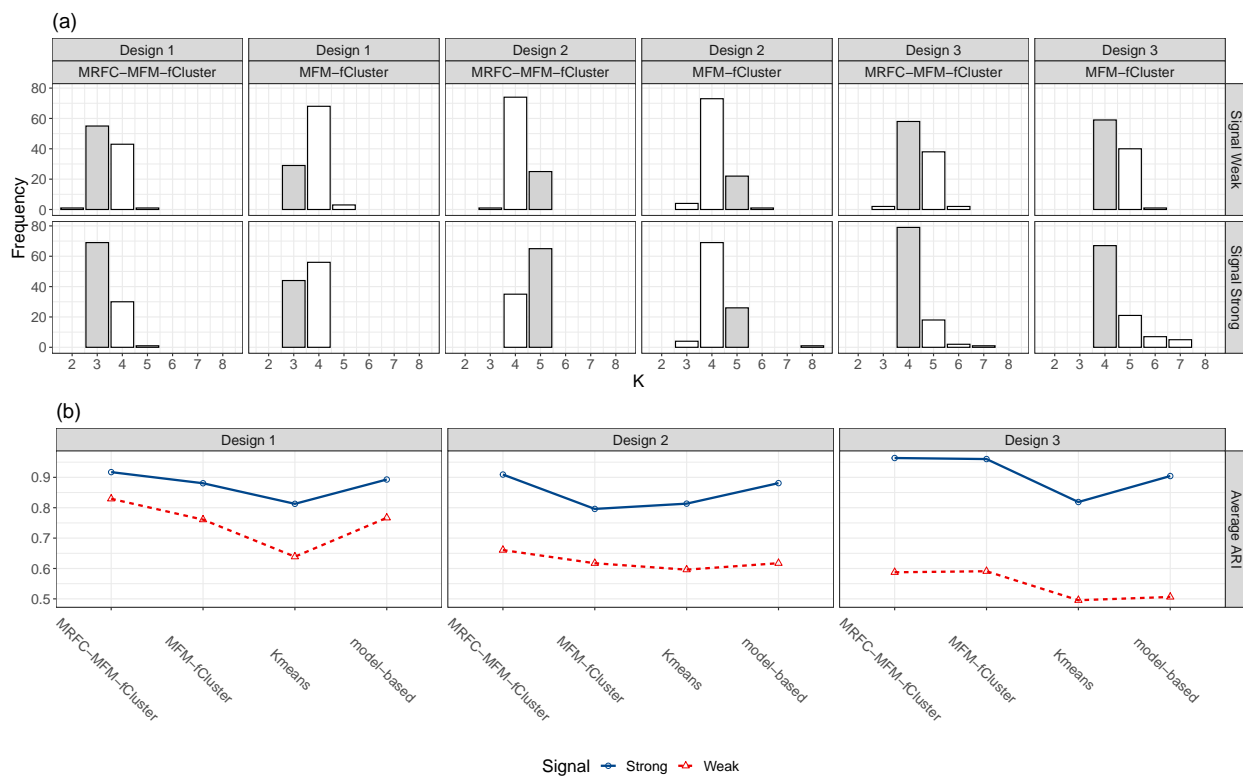


Figure 7: (a) Histogram of number of clusters inferred by MRFC-MFM-fCluster and MFM-fCluster under different designs and signal strength settings. The grey bars correspond to the correct number of clusters. (b) Plot of ARIs for all four methods under different designs and signal strength settings.

Table 2: Average  $\lambda$  selected by mDIC for 100 simulation replicates for each combination of signal strength and true cluster design.

	Design 1	Design 2	Design 3
Signal Weak	1.535	1.715	1.630
Signal Strong	1.680	1.630	1.610

Performances are visualized in Figure 7, and the average optimal  $\lambda$ 's selected by mDIC are presented in Table 2. In Figure 7(a), it can be seen that under design 1, MFM-fCluster exhibits severe over-clustering, which produces four final clusters for more than 60 replicates under the weak signal setting, and more than 50 replicates in the strong signal setting. In contrast, even under the weak signal setting, MRFC-MFM-fCluster is able to correctly infer the true number of clusters for more than 50 replicates, and a notable number of 69 for strong signal. Under design 2, as cluster sizes are relatively small, it is rather difficult for both MRFC-MFM-fCluster and MFM-fCluster to infer the number of clusters under the weak signal setting, as can be seen from the top middle two plots. With strong signal, however, MRFC-MFM-fCluster is able to correctly identify the true number of clusters for more than half of simulation replicates, while the performance of MFM-fCluster remains poor. Under design 3, as the true clusters are “messy” in the sense that there are no clear spatially contiguous states that belong to the same cluster, the performance of MRFC-MFM-fCluster is similar to that of MFM-fCluster in the weak signal setting. With strong signal, however, MFM-fCluster again overclusters, producing for 67 replicates the correct  $K$ , while this number for MRFC-MFM-fCluster is 79. In Figure 7(b), our proposed method has the highest average ARI over 100 replicates for all six combinations of signal and partition design. The model-based functional clustering has the second best performance in designs 1 and 2, and the third best performance in design 3, while MFM-fCluster has the second best performance in design 3, and the third best in designs 1 and 2. In all cases,  $K$ -means performs the worst.

In addition, computation times for all methods are benchmarked using R package **microbenchmark** (Mersmann, 2019) on a desktop computer running Windows 10 Enterprise, with i7-8700K CPU@3.70GHz using single-core mode. A total of 20 replicates are performed to compute the average running time for each method. As expected,  $k$ -means takes the least time of 1.62 seconds due to its simple iterative algorithm. Unlike the  $k$ -means which can only provide clusters without making statistical inference of cluster memberships and sizes, our proposed method utilizes conjugate forms for efficient Bayesian inference that provides not only estimates of clusters but also their uncertainty measures at only a slightly higher computation cost. Indeed, it takes on average 20.79 seconds for one simulated dataset with 500 MCMC iterations, as in our empirical studies 500 iterations are sufficient for the chain to converge and stabilize. The model-based approach, however, takes more than three minutes to finish. Due to the time-consuming nature of the model-based approach, the actual simulation studies are conducted on a 16-core desktop computer using parallel computation. The code is submitted for review and will be made publicly available at GitHub after the acceptance of the manuscript.

## 6 Analysis of PUMS Data

In this section, we apply the proposed MRFC-MFM-fCluster to the analysis of US households' income in 2017. Similar as in the simulation studies, the Lorenz curves for all states are obtained for the functional clustering analysis. Based on (3.1) and (3.2), we get the inner product matrix  $\mathbf{S}$ . The spatial smoothing parameter  $\lambda$  is considered within the range of  $\{0, 0.2, 0.4, \dots, 3\}$ , with  $\lambda = 0$  corresponding to MFM-fCluster. The upper limit for considering a state "neighbor" is considered within the range  $\{1, 2, 3\}$ . The mDIC is used to determine the optimal combination of these two parameters. From the sensitivity analyses presented in the supplemental material,  $\gamma$  values are not particularly impactful on the clustering performance, and thus it is set to be consistent with in the simulation studies

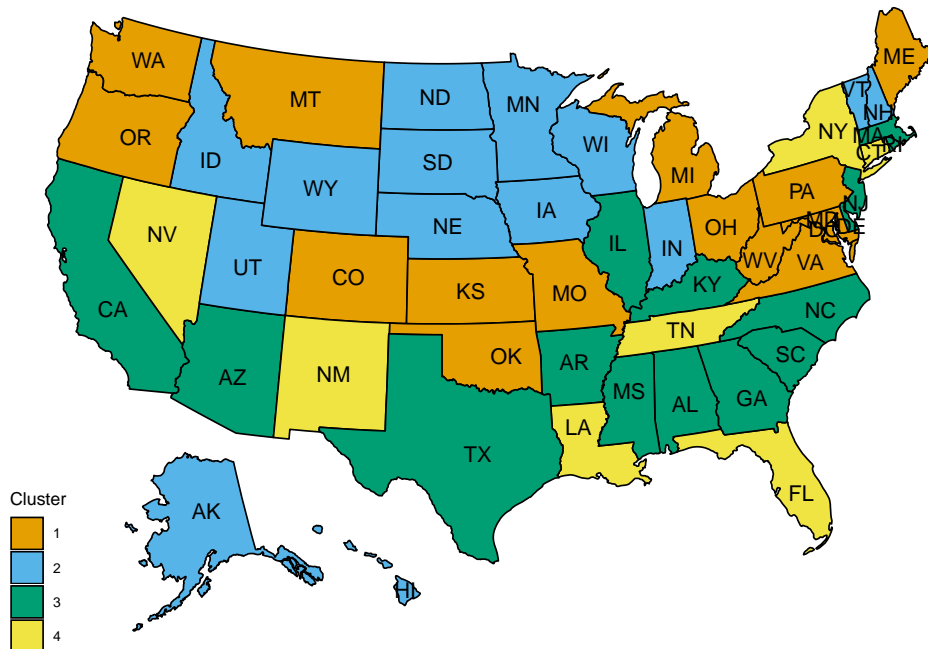


Figure 8: Illustration of the four clusters identified by the proposed method for the 51 states.

described in Section 4.1. We choose following hyperparameters  $\alpha = 1$  and  $\beta = 1$  which are consistent with our simulation studies.

The final model selected corresponding to the smallest mDIC value has  $\lambda = 0.8$  and upper limit 2 for defining neighbors. The final cluster configuration is visualized in Figure 8. There are, respectively, 14, 14, 15 and 8 states in clusters 1, 2, 3 and 4. Cluster 4 tops in terms of income inequality, and has an average Gini coefficient of 0.491. Cluster 2, with an average Gini of 0.435, exhibits the most equal income distribution among the four. Clusters 1 and 3 have average Gini values of 0.458 and 0.477.

One particularly important merit of our proposed method is that it allows for globally discontinuous clusters. As shown in Figure 8, New Mexico and Tennessee belong to the same cluster. Their 2017 Gini coefficients are 0.4851 and 0.4858, respectively, which indicates these two states have very similar IDs in terms of Gini coefficients. Based on 2010 American Community Survey from U.S. Census Bureau <https://factfinder.census.gov/>, the Gini coefficients of these two states have been historically very close. In addition, there are several

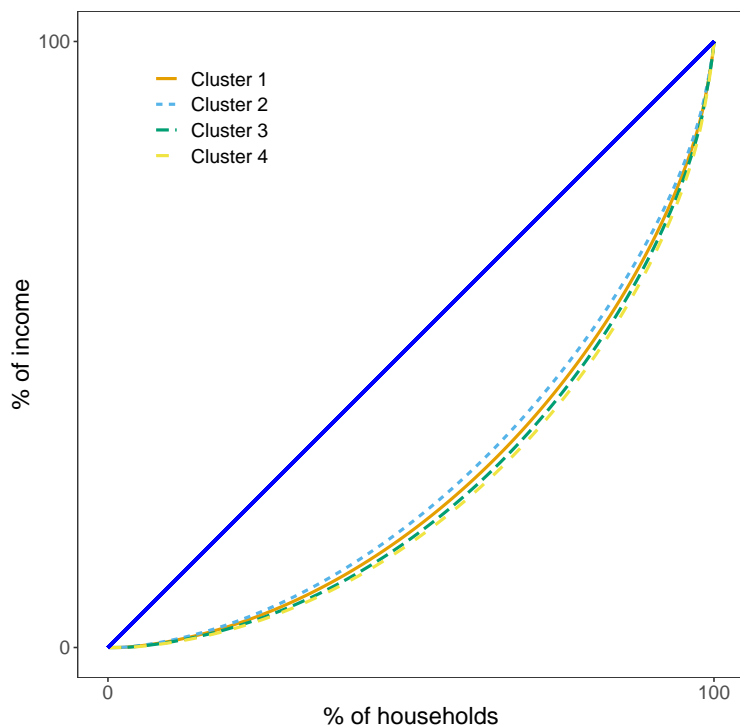


Figure 9: Average Lorenz curves for states in the four identified clusters.

government policies that could be applied for different clusters. For the states in Clusters 3 and 4, increasing the minimum wage and expanding the earned income tax are two strategies for improving the equality of ID. Most states in Cluster 1 have much lower median household income. Decreasing the income tax will help increase their overall household income, which is at the cost of minor sacrifice in ID equality. Furthermore, an increase in government expenditures will help increase the household income directly for the states in Cluster 1. For the states in Cluster 2, they have most balanced ID and mid-level median household income. Most their government policies can be kept for steady economy growth. From the clustering results, we still find that the states with large metropolitan areas tend to have less balanced IDs, which is consistent with the findings in [Glassman and Branch \(2017\)](#). Based on the results shown in [Janikas et al. \(2005\)](#); [Rey \(2018\)](#) which analyzed the income data collected from the Bureau of Economic Analysis, they claimed that the states with high (low) levels of internal inequality tend to be located next to other states with high (low) levels of inequality.

This claim confirms our spatial homogeneity patterns of IDs among different states. Taking Cluster 1 and Cluster 2 as examples, these two clusters have a large number of states sharing the same boundary, since they have low levels of internal inequality.

The posterior estimate of  $\mathbf{U}$  in (3.16) is

$$\hat{\mathbf{U}} = \begin{pmatrix} 4.885 & 4.186 & 4.293 & 3.692 \\ 4.186 & 4.700 & 3.710 & 3.341 \\ 4.293 & 3.710 & 4.821 & 4.042 \\ 3.692 & 3.341 & 4.042 & 4.524 \end{pmatrix}. \quad (6.1)$$

It is noticeable that the diagonal entries of  $\mathbf{U}$  are larger than the off-diagonal entries, which suggests the within-cluster similarity is much higher than between-clusters similarities. Cluster 1 has least similarity with Cluster 4 based on (6.1), which is consistent with the results presented in Figure 9.

Finally, to make sure the cluster configuration presented here is not a random occurrence but reflects the true pattern demonstrated by the data, we run 100 separate MCMC chains with different random seeds and initial values, and obtained 100 final clustering schemes. The RI between each scheme and the present clustering scheme in Figure 8 is calculated, and they average to 0.899, indicating high concordance of conclusion regardless of random seeds. As suggested by a reviewer, we also use the sequentially-allocated latent structure optimization (SALSO) algorithm implemented in the R package `salso` (Dahl, 2020) to check for uncertainties in the presented clustering result. The details are included in Section 4 of the supplemental material.

## 7 Discussion

In this paper, we proposed both mixture of finite mixtures (MFM) and Markov random field constrained mixture of finite mixtures (MRFC-MFM) to capture spatial homogeneity of ID

based on functional inner product of Lorenz curves. Two efficient algorithms are proposed for the inference of the proposed methods. Parameter tuning is achieved using a modified version of DIC, the popular Bayesian model selection criterion. Comprehensive simulation studies are carried out to show MRFC-MFM achieves better performance than the traditional MFM model in terms of spatial homogeneity pursuit. It also outperforms the  $K$ -means and model-based methods under various designs, and the comparison of performance is relatively robust under different choices of the spatial smoothing parameters. A case study using the PUMS data reveals a number of important findings of IDs across 51 states in US.

A few topics beyond the scope of this paper are worth further investigation. In this paper, Fisher’s  $Z$ -transformation of the inner product matrix is used. Modeling the original inner product matrix is an interesting alternative in future work. Independence is assumed between elements of the inner product matrix  $\mathbf{S}$  for modeling and computation simplicity and convenience, and extending SBM to incorporate such edge dependence similar to [Yuan and Qu \(2018\)](#) is an interesting but nontrivial problem devoted for future research. In addition, tuning of  $\lambda$  is criterion-based. Treating it as an unknown parameter and proposing a prior in a hierarchical model for it may improve the efficiency. Besides the geographical information, other auxiliary covariates, such as demographic information, could also be taken into account for clustering in our future work. While our clustering methods are based on similarity matrix or dissimilarity matrix, the proposed MRFC-MFM clustering prior model can be adapted to other hierarchical model settings, including the case with multiple similarity matrices as responses ([Paul et al., 2016](#); [Lei et al., 2020](#)) Extending our prior on functional data model with basis coefficients ([Suarez et al., 2016](#)) is also another interesting future work.



## A Proof of Theorem 3.1

Full conditionals  $\Pi(\boldsymbol{\theta}_i | \boldsymbol{\theta}_{-i})$  from (3.15) can be obtained up to a constant as the product of the full conditionals of each part

$$\begin{aligned}
\Pi(\boldsymbol{\theta}_i | \boldsymbol{\theta}_{-i}) &\propto P(\boldsymbol{\theta}_i | \boldsymbol{\theta}_{-i})M(\boldsymbol{\theta}_i | \boldsymbol{\theta}_{-i}) \\
&\propto M(\boldsymbol{\theta}_i | \boldsymbol{\theta}_{-i}) \sum_{k=1}^{K^*} (n_k^{(-i)} + \gamma) \delta_{\boldsymbol{\theta}_k^*} + M(\boldsymbol{\theta}_i | \boldsymbol{\theta}_{-i}) \frac{V_n(K^* + 1)}{V_n(K^*)} \gamma G_0(\boldsymbol{\theta}_i) \\
&\propto M(\boldsymbol{\theta}_i | \boldsymbol{\theta}_{-i}) \sum_{k=1}^{K^*} (n_k^{(-i)} + \gamma) \delta_{\boldsymbol{\theta}_k^*} + \frac{1}{Z_H} \frac{V_n(K^* + 1)}{V_n(K^*)} \gamma G_0(\boldsymbol{\theta}_i) \tag{A.1} \\
&\propto \sum_{k=1}^{K^*} (n_k^{(-i)} + \gamma) \frac{1}{Z_H} \exp(-H(\boldsymbol{\theta}_i | \boldsymbol{\theta}_{-i})) \delta_{\boldsymbol{\theta}_k^*}(\boldsymbol{\theta}_i) + \frac{V_n(K^* + 1)}{V_n(K^*)} \frac{\gamma}{Z_H} G_0(\boldsymbol{\theta}_i)
\end{aligned}$$

As a direct characteristic from the defined cost function  $H$  in (3.14), the support of  $H$  is the set of existing cluster parameters  $\boldsymbol{\theta}_1^*, \dots, \boldsymbol{\theta}_{K^*}^*$ . When  $\boldsymbol{\theta}_i$  is generated from the base distribution  $G_0$ ,  $H(\boldsymbol{\theta}_i | \boldsymbol{\theta}_{-i}) = 0$  and  $M(\boldsymbol{\theta}_i | \boldsymbol{\theta}_{-i}) = \frac{1}{Z_H}$ . This results in the derivation from the second to the third step above.

The last step is simply to plug in  $M(\boldsymbol{\theta}_i | \boldsymbol{\theta}_{-i})$  from its definition.

## References

- Akaike, H. (1973). Information theory and an extension of the maximum likelihood principle. In B. N. Petrov and F. Csaki (Eds.), *Second International Symposium on Information Theory*, pp. 267–281. Akadémiai Kiado. [20](#)
- Aldous, D. J. (1985). Exchangeability and related topics. In *École d'Été de Probabilités de Saint-Flour XIII—1983*, pp. 1–198. Springer. [13](#)
- Antoniak, C. E. (1974). Mixtures of Dirichlet processes with applications to Bayesian non-parametric problems. *The Annals of Statistics* 2(6), 1152–1174. [12](#)

- Bartels, C. P. and H. Van Metelen (1975). *Alternative Probability Density Functions of Income: A Comparison of the Lognormal-, Gamma-and Weibull-distribution with Dutch Data*. Vrije Universiteit, Economische Faculteit. [3](#)
- Bhattacharyya, S. and P. J. Bickel (2014). Community detection in networks using graph distance. *arXiv preprint arXiv:1401.3915*. [23](#)
- Blackwell, D., J. B. MacQueen, et al. (1973). Ferguson distributions via Pólya urn schemes. *The Annals of Statistics* 1(2), 353–355. [12](#), [13](#)
- Borchers, H. W. (2019). *pracma: Practical Numerical Math Functions*. R package version 2.2.9. [10](#)
- Cowell, F. A. and M.-P. Victoria-Feser (2008). Modelling Lorenz curves: Robust and semi-parametric issues. In *Modeling Income Distributions and Lorenz Curves*, pp. 241–253. Springer. [3](#)
- Dahl, D. B. (2006). Model-based clustering for expression data via a Dirichlet process mixture model. In M. V. Kim-Anh Do, Peter Müller (Ed.), *Bayesian Inference for Gene Expression and Proteomics*, Volume 4, pp. 201 – 218. Cambridge University Press. [19](#)
- Dahl, D. B. (2020). *salso: Sequentially-Allocated Latent Structure Optimization*. R package version 0.1.16. [31](#)
- Gastwirth, J. L. (1972). The estimation of the Lorenz curve and Gini index. *The Review of Economics and Statistics* 54(3), 306–316. [7](#)
- Geman, S. and D. Geman (1984). Stochastic relaxation, Gibbs distributions, and the Bayesian restoration of images. *IEEE Transactions on Pattern Analysis and Machine Intelligence PAMI-6*(6), 721–741. [15](#)

- Geng, J., A. Bhattacharya, and D. Pati (2019). Probabilistic community detection with unknown number of communities. *Journal of the American Statistical Association* 114(526), 893–905. [14](#)
- Gibrat, R. (1931). *Les inégalités économiques*. Recueil Sirey. [3](#)
- Gini, C. (1997). Concentration and dependency ratios. *Rivista di Politica Economica* 87, 769–792. [2](#)
- Giraldo, R., P. Delicado, and J. Mateu (2012). Hierarchical clustering of spatially correlated functional data. *Statistica Neerlandica* 66(4), 403–421. [4](#)
- Glassman, B. and P. S. Branch (2017). Income inequality among regions and metropolitan statistical areas: 2005 to 2015. Technical report, U.S. Census Bureau. [30](#)
- Heaton, M. J., W. F. Christensen, and M. A. Terres (2017). Nonstationary Gaussian process models using spatial hierarchical clustering from finite differences. *Technometrics* 59(1), 93–101. [5](#)
- Holland, P. W., K. B. Laskey, and S. Leinhardt (1983). Stochastic blockmodels: First steps. *Social Networks* 5(2), 109–137. [11](#)
- Hoover, E. M. (1936). The measurement of industrial localization. *The Review of Economic Statistics*, 162–171. [3](#)
- Hubert, L. and P. Arabie (1985). Comparing partitions. *Journal of Classification* 2(1), 193–218. [20](#)
- Jacques, J. and C. Preda (2014). Functional data clustering: A survey. *Advances in Data Analysis and Classification* 8(3), 231–255. [3](#)
- James, G. M. and C. A. Sugar (2003). Clustering for sparsely sampled functional data. *Journal of the American Statistical Association* 98(462), 397–408. [25](#)

- Janikas, M. V., S. J. Rey, et al. (2005). Spatial clustering, inequality and income convergence. *Région et Développement* 21(2), 45–64. [30](#)
- Jiang, H. and N. Serban (2012). Clustering random curves under spatial interdependence with application to service accessibility. *Technometrics* 54(2), 108–119. [4](#)
- Kim, H.-M., B. K. Mallick, and C. C. Holmes (2005). Analyzing nonstationary spatial data using piecewise Gaussian processes. *Journal of the American Statistical Association* 100(470), 653–668. [4](#)
- Knorr-Held, L. and G. Raßer (2000). Bayesian detection of clusters and discontinuities in disease maps. *Biometrics* 56(1), 13–21. [4](#)
- Lee, J., R. E. Gangnon, and J. Zhu (2017). Cluster detection of spatial regression coefficients. *Statistics in Medicine* 36(7), 1118–1133. [4](#)
- Lei, J., K. Chen, and B. Lynch (2020). Consistent community detection in multi-layer network data. *Biometrika* 107(1), 61–73. [32](#)
- Li, F. and H. Sang (2019). Spatial homogeneity pursuit of regression coefficients for large datasets. *Journal of the American Statistical Association* 114(527), 1050–1062. [4](#)
- Lorenz, M. O. (1905). Methods of measuring the concentration of wealth. *Publications of the American Statistical Association* 9(70), 209–219. [2](#), [6](#)
- Mankiw, N. G. (2014). *Principles of Economics*. Cengage Learning. [2](#)
- McDonald, J. B. (1984). Some generalized functions for the size distribution of income. *Econometrica: Journal of the Econometric Society* 52(3), 647–663. [3](#)
- McDonald, J. B. and Y. J. Xu (1995). A generalization of the Beta distribution with applications. *Journal of Econometrics* 66(1), 133–152. [3](#)

- Mersmann, O. (2019). *microbenchmark: Accurate Timing Functions*. R package version 1.4-7. [28](#)
- Miller, J. W. and M. T. Harrison (2018). Mixture models with a prior on the number of components. *Journal of the American Statistical Association* 113(521), 340–356. [5](#), [13](#), [14](#), [17](#), [18](#)
- Neal, R. M. (2000). Markov chain sampling methods for Dirichlet process mixture models. *Journal of Computational and Graphical Statistics* 9(2), 249–265. [12](#), [13](#)
- Orbanz, P. and J. M. Buhmann (2008). Nonparametric Bayesian image segmentation. *International Journal of Computer Vision* 77(1-3), 25–45. [15](#)
- O’sullivan, A. and S. M. Sheffrin (2007). *Prentice Hall Economics: Principles in Action*. Pearson/Prentice Hall. [2](#)
- Pareto, V. (1964). *Cours d’économie Politique*, Volume 1. Librairie Droz. [3](#)
- Paul, S., Y. Chen, et al. (2016). Consistent community detection in multi-relational data through restricted multi-layer stochastic blockmodel. *Electronic Journal of Statistics* 10(2), 3807–3870. [32](#)
- Pitman, J. (1995). Exchangeable and partially exchangeable random partitions. *Probability Theory and Related Fields* 102(2), 145–158. [13](#)
- Rand, W. M. (1971). Objective criteria for the evaluation of clustering methods. *Journal of the American Statistical Association* 66(336), 846–850. [20](#)
- Rey, S. J. (2018). Bells in space: The spatial dynamics of us interpersonal and interregional income inequality. *International Regional Science Review* 41(2), 152–182. [30](#)
- Romano, E., R. Verde, and V. Cozza (2011). Clustering spatial functional data: A method based on a nonparametric variogram estimation. In S. Ingrassia, R. Rocci, and M. Vichi

(Eds.), *New Perspectives in Statistical Modeling and Data Analysis*, pp. 339–346. Springer.

[4](#)

Ryu, H. K. and D. J. Slottje (1996). Two flexible functional form approaches for approximating the Lorenz curve. *Journal of Econometrics* 72(1-2), 251–274. [3](#)

Salem, A. B. and T. D. Mount (1974). A convenient descriptive model of income distribution: the Gamma density. *Econometrica: Journal of the Econometric Society* 42(6), 1115–1127.

[21](#)

Schwarz, G. et al. (1978). Estimating the dimension of a model. *The Annals of Statistics* 6(2), 461–464. [20](#)

Scrucca, L., M. Fop, T. B. Murphy, and A. E. Raftery (2016). mclust 5: Clustering, classification and density estimation using Gaussian finite mixture models. *The R Journal* 8(1), 289–317. [23](#)

Spiegelhalter, D. J., N. G. Best, B. P. Carlin, and A. Van Der Linde (2002). Bayesian measures of model complexity and fit. *Journal of the Royal Statistical Society: Series B (Methodological)* 64(4), 583–639. [20](#)

Srivastava, A., E. Klassen, S. H. Joshi, and I. H. Jermyn (2010). Shape analysis of elastic curves in Euclidean spaces. *IEEE Transactions on Pattern Analysis and Machine Intelligence* 33(7), 1415–1428. [9](#), [10](#)

Srivastava, A. and E. P. Klassen (2016). *Functional and Shape Data Analysis*. Springer. [5](#)

Suarez, A. J., S. Ghosal, et al. (2016). Bayesian clustering of functional data using local features. *Bayesian Analysis* 11(1), 71–98. [4](#), [32](#)

Tucker, J. D. (2019). *fdasrvf: Elastic Functional Data Analysis*. R package version 1.9.2. [10](#)

Tucker, J. D., W. Wu, and A. Srivastava (2013). Generative models for functional data using phase and amplitude separation. *Computational Statistics & Data Analysis* 61, 50–66. [10](#)

- Winkler, G. (2012). *Image Analysis, Random Fields and Markov Chain Monte Carlo Methods: A Mathematical Introduction*, Volume 27. Springer Science & Business Media. [15](#)
- Yuan, Y. and A. Qu (2018). Community detection with dependent connectivity. *arXiv preprint arXiv:1812.06406*. [32](#)
- Zhang, Z., D. Pati, and A. Srivastava (2015). Bayesian clustering of shapes of curves. *Journal of Statistical Planning and Inference* 166, 171–186. [10](#)